Characterization of the short Hydrogen Beam setup

Martin Roelfs
Supervisor: Chloé Malbrunot

***Abstract*—As part of the CERN summer student program I participated in building a short hydrogen beamline. After completion of the assembly my work consisted of characterization of the beamline.**

A so-called chopper is used for modulating the beam in order to distinguish the beam from the background hydrogen in the vacuum chambers. This modulation is also used to measure the velocity of the beam via a Time-of-Flight (TOF) measurement. It was found that the extracted velocity is dependent on the driving voltage of the chopper.

Upstream of the chopper a pair of permanent sextupoles is used for polarizing the beam and velocity selection. The effect of the relative separation of these sextupoles on the velocity distribution was also investigated as part of this report.

I. Introduction

For the past 13 weeks I worked as a summer student in the ASACUSA collaboration. Parallel to the ASACUSA experiment's efforts to measure the hyperfine splitting in anti-hydrogen, a hydrogen beamline was build last year and successfully measured one of the hyperfine transitions in hydrogen. After improvements, this setup is now being rebuild in order to measure a second transition in hydrogen. This is being done in three stages, and the project is now entering it's second stage. As part of my project, I helped build and characterize the first stage, and am currently building the second stage.

The transition this experiment is trying to measure is caused by the coupling of the proton and electron spin in the (anti)hydrogen atom. The spin states can combine to form two different energy states, and the energy difference is known as the hyperfine splitting. This is illustrated in Figure 1.

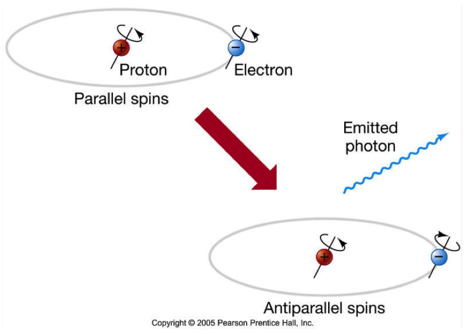

Fig. 1: Emission of a 21 cm photon as a result of hyperfine splitting.

The coupling of the electron and proton in the hydrogen atom can give either a singlet or a triplet state.

If an external magnetic field is applied to the hydrogen atom, the degeneracy of the triplet state is broken and the states are no longer equivalent. This behavior is depicted in Figure 2a, and is known as the Zeeman effect.

The breaking of the degeneracy allows for polarization of the beam using a magnetic field gradient. As can be seen from the energy diagram in Figure 2a, for some states a low magnetic field is energetically favorable while for others a high field is preferable. Therefore, by applying an homogeneous magnetic field the beam gets polarized. As can be seen in Figure 2b, an ideal sextupole has zero field in the center, making it focus states that prefer low field

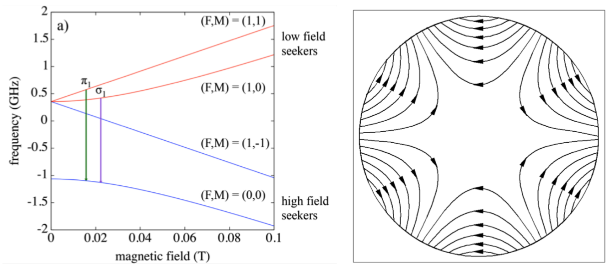

(a) (b)

Fig. 2: Left: If an external magnetic field is applied, the triplet states are no longer degenerate, an effect known as the Zeeman effect. Right: An ideal sextupole field is zero in the center, making it ideal for polarizing a beam of mixed spin states in this experiment because it focuses the low field seekers. Image credit: cds.cern.ch.

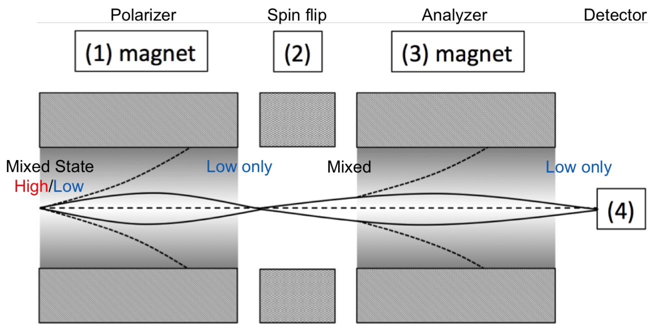

Fig. 3: (1) Polarizing sextupole. Selects low field seeking states only. (2) Spin-flip cavity. When near resonance this flips part of the low field seekers into high field seekers. (3) Analyzing sextupole. This selects for low field seekers again. (4) Detector to count the number of particles left after the analyzing sextupole. When on resonance, the count rate should decrease.

while defocusing high field preferring states. It focuses independent of the velocity of the beam, making a sextupole field ideal for our experiment.

The experiment takes advantage of the Zeeman effect in order to measure the resonance frequency. The concept is illustrated in Figure 3 and is similar to polarization experiments in optics. The first sextupole acts as a polarizer, leaving only the low field seeking states. The second sextupole acts as an analyzer, again leaving only the low field seeking states. If in between the two sextupoles a spin-flip is induced, a drop in signal is expected since part of the low field seekers are transformed into high field seekers and these are defocused at the analyzer.

Therefore a drop in signal is expected when the resonance frequency is found, giving an accurate way to measure the resonance frequency of the hyperfine splitting.

The full setup is illustrated in Figure 4.

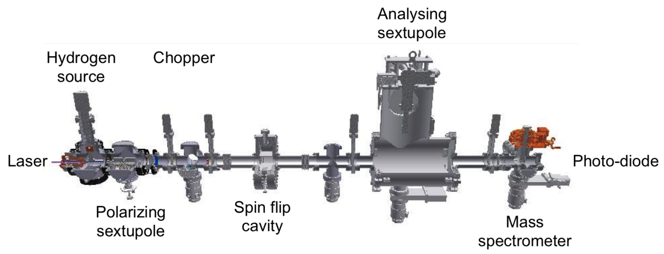

Fig. 4: Hydrogen beam setup.

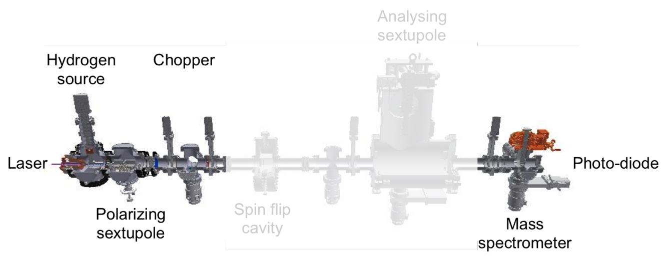

Fig. 5: Short hydrogen beam setup. Connects the hydrogen source to the mass spectrometer via the polarizing sextupole and the chopper chamber.

II. Method & Results

The first characterization stage consists of a shorter setup, as illustrated in Figure 5. Helping to build this setup was the biggest part of the project, followed by characterization of the setup. The short setup consists of the following parts:

Laser/Photo-diode A laser beam is pointed straight through the entire setup at a photo-diode. The shape of the photo-diode signal reflects the motion of the chopper and is used for data analysis. See Section II-C2 for more details.

Hydrogen source In order to create atomic hydrogen, a hydrogen plasma is created. The resultant particles are then guided into the setup and cooled to cryogenic temperatures as it hits the surface of Teflon tubing cooled by liquid helium..

Polarizing sextupole Polarizes the hydrogen beam and is designed to do a velocity selection. For a more detailed description, see Section II-A.

Chopper Modulates the beam by cutting it with a frequency of 178 Hz. This allows for characterization of the velocity of the beam.

Mass spectrometer A Quadrupole Mass Spectrometer (QMS) is used to measures the rate of ^{1}H at the detector.

In the characterizations that follow, a Time Of Flight (TOF) measurement is performed in order to obtain the velocity of the beam. In order to perform such a measurement, the beam is cut by the chopper. Therefore, while the chopper is open particles go through with a distribution of velocities. The signal arriving at the QMS is a convolution of the chopper function and the velocity distribution. An example of such a signal is given in Figure 6.

It is hypothesized that the polarizing sextupole generates a Gaussian velocity distribution rather than a Maxwell-Boltzmann distribution. Therefore the quality of fit for these two models was tested.

Furthermore, the influence of the separation in the polarizing sextupole on the velocity distribution was investigated, as well as the effect of chopper amplitude.

A. Distribution Type

1) Method: The polarizing sextupole consists of two halves with an adjustable spacing between them as shown in Figure 7a. The spacing is expressed in mounting hole number, as in the experiment the separation is set by selecting a mounting hole. In an internal study simulations were carried out which indicate that the separation of the sextupoles allows for velocity selection. The simulations show that assuming a Maxwell-Boltzmann distribution at the source, the sextupole selects a Gaussian shaped part of the distribution.

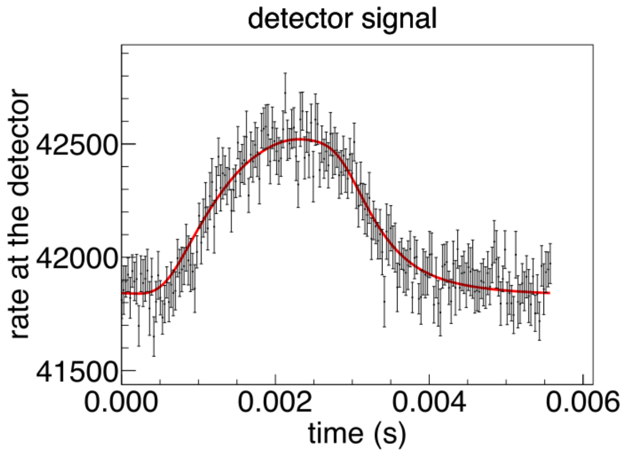

Fig. 6: Example of TOF data fitted with the convolution of a Gaussian and the photo-diode signal.

Voltage	Model	χ^2/dof	v / ms^{-1}	σ_v / ms^{-1}	T/K
0.88	Gaussian	1.70	573.1 $\pm$ 38.2	122.7 $\pm$ 29.2	13.8
	M-B	1.71	525.9	221.9	13.1
1.92	Gaussian	1.85	609.3 $\pm$ 22.8	11.1 $\pm$ 18.4	15.4
	M-B	1.97	596.0	251.5	16.8
3.48	Gaussian	2.02	705.7 $\pm$ 19.7	198.0 $\pm$ 12.9	21.5
	M-B	2.07	568.1	239.8	15.2
4.56	Gaussian	2.62	757.7 $\pm$ 17.4	219.3 $\pm$ 11.3	24.9
	M-B	2.74	598.3	252.5	16.9
5.60	Gaussian	2.41	750.2 $\pm$ 18.7	218.4 $\pm$ 13.2	24.5
	M-B	2.64	592.9	250.2	16.6
7.48	Gaussian	2.13	693.1 $\pm$ 17.0	182.7 $\pm$ 10.9	20.6
	M-B	2.29	584.2	246.5	16.1

TABLE I: Fits of a Gaussian and Maxwell-Boltzmann distributions convoluted with the photo-diode signal. 20K, mounting hole 27.

To test this, a convolution of either a Gaussian or a Maxwell-Boltzmann distribution with the photo-diode signal were fitted to the chopper data used in Section II-C2 to test which describes the data better. In order to distinguish the models a chi-squared test is performed and the temperature of the distributions is compared.

The temperature of a Gaussian distribution is calculated by using the familiar expression

$$\frac{3}{2}k_B T = \langle \frac{1}{2} m_H v^2 \rangle = \frac{1}{2} m_H \langle v^2 \rangle \quad (1)$$

$$T = \frac{m_H}{3k_B} \langle v^2 \rangle \quad (2)$$

Here a monoatomic beam of atomic hydrogen is assumed. For a Gaussian distribution $\langle v^2 \rangle$ is the second moment of the distribution, given by

$$\langle v^2 \rangle = \langle v \rangle^2 + \sigma_v^2 \quad (3)$$

2) Results: Table I lists the results. A Chi-squared test does not allow to distinguish between the two models, since both models give similar χ^2 values.

The only promising result is the temperature of the fitted distribution. The source is set to 20K, and with mounting hole 27 one would

(a) Polarizing Sextupole, with spacing between the two halves.

(b) CH-10 Tuning Fork Chopper.

Fig. 7

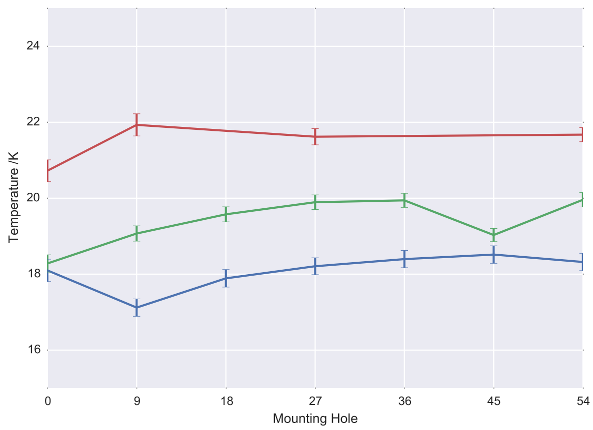

Fig. 8: Mounting hole vs Temperature.

expect to select faster particles. The Maxwell-Boltzmann model gives temperatures that don't match with these conditions. Therefore the Maxwell-Boltzmann model can be excluded whereas the Gaussian model can not be excluded. Further study is needed, in particular a full reanalysis of the mounting hole scan with both distributions.

B. Mounting Hole Scan

1) Method: Measurements were performed to test if a higher mounting hole increases the velocity of the beam as suggested by simulations and earlier hyperfine splitting measurements performed with the full setup. This was done by measuring mounting holes 0 through 54 in steps of nine. After each measurement a reference measurement at mounting hole 27 was performed to be able to correct for drifts.

Additionally this scan was repeated at 20K, 40K and 60K to test the dependence on source temperature.

2) Results: The results are shown in Figure 8. The TOF fit to the mounting hole data was performed using a Gaussian convoluted with the photo-diode signal as the fit function.

No clear dependence on mounting hole is visible, and there only appears to be a small but systematic dependence on the source temperature. Since this measurement was performed in the center of the beam one would expect the part of the beam that passes through the center of the magnet to be undisturbed, and therefore to reflect the source temperature. This does not seem to be the case as strongly as one would expect. To investigate this further, a 2D scan of the beam profile as it arrives at the QMS was performed. The result is displayed in Figure 9.

The phase difference is a first order measure of the velocity. From this it appears that:

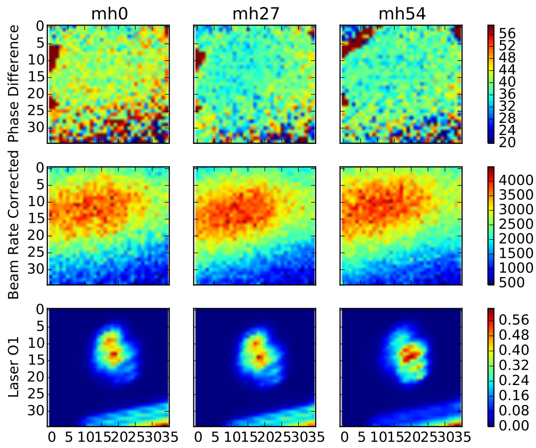

Fig. 9: 2D scan of the beam profile at the QMS. Top row: phase difference between beam and laser signal. This is a first order measure of velocity. Middle row: count rate. Bottom row: photo-diode signal.

- the velocity distribution is quite homogeneous over the beam
- the velocity for mounting hole 27 and mounting hole 54 appear similar
- the difference between 0 and 27 appears to be small

A potential explanation for the lack of mounting hole dependence is the defocusing of the beam as caused by the sextupole. This can be tested with the long setup (Section III).

C. Chopper Characterization

1) Method: The chopper cuts the beam in order to allow for signal modulation. The chopper device is depicted in Figure 7b. The chopper is driven by a sinusoidal signal, but is closed for half of the signal when the scissors overlap. Ideally then, if a laser is pointed through the chopper half a sine would be obtained for the first half of the period, and no signal for the second half.

In order to characterize the effect of the chopper amplitude the count rate at the QMS is measured, as is the laser intensity. As mentioned in II-B, we assume the polarizing sextupole to select a Gaussian shaped subsection of the velocity distribution. In order to quantify the effect of the chopper amplitude either a half sine or the photo-diode signal was convoluted with a Gaussian distribution and fitted to the count rate at the QMS detector.

2) Results: Figure 10 shows the laser signal measured as a function of amplitude. It is clear that as the amplitude becomes higher, a half-sine no longer accurately describes the chopper's motion.

The beam was produced with a temperature of 20K, at mounting hole position 27. In the beam counts as shown on the left in Figure 10 the chopper shape is visible. However, it is convoluted with the velocity distribution of the beam. Since the velocity of the beam is the property of interest, it is proposed to use the chopper signal as measured by the photo-diode instead of an idealization when fitting to the beam counts.

In order to compare, a Gaussian distribution convoluted with either a half-sine or the photo-diode data was fitted to the corrected beam counts. The results are listed in Table II. When using the half sine the following observations can be made about the results: firstly, the velocity obtained shows a dependence on the chopper amplitude. Secondly, the errors in the fit parameters show a large dependence on the chopper amplitude. A chopper amplitude of about 3.48 V seems optimal when using a sine shaped fit.

Voltage	Half sine χ^2/dof	v / ms^{-1}	σ_v / ms^{-1}	T/K	Photo-diode χ^2/dof	v / ms^{-1}	σ_v / ms^{-1}	T/K
0.88	1.76	451.9 ± 352.9	703.8 ± 345.9	28.0	1.70	573.1 ± 38.2	122.7 ± 29.2	13.7
1.92	1.85	445.7 ± 54.2	146.1 ± 277.7	8.8	1.85	609.3 ± 22.8	112.1 ± 18.4	15.4
3.48	1.82	533.7 ± 13.4	138.8 ± 108.6	12.2	2.02	705.7 ± 19.7	198.0 ± 12.9	21.5
4.56	2.45	554.3 ± 97.8	147.3 ± 753.9	13.2	2.62	757.7 ± 17.4	219.3 ± 11.3	24.9
5.60	1.99	508.6 ± 101.9	109.9 ± 97.4	10.8	2.41	750.2 ± 18.7	218.4 ± 13.2	24.5
7.48	2.09	529.8 ± 961.9	133.7 ± 706.7	12.0	2.13	693.1 ± 17.0	182.7 ± 10.9	20.6

TABLE II: Fits of a Gaussian distribution convoluted with either a half-sine or the chopper function as obtained from the photo-diode signal. Voltages are peak to peak as measured with an oscilloscope.

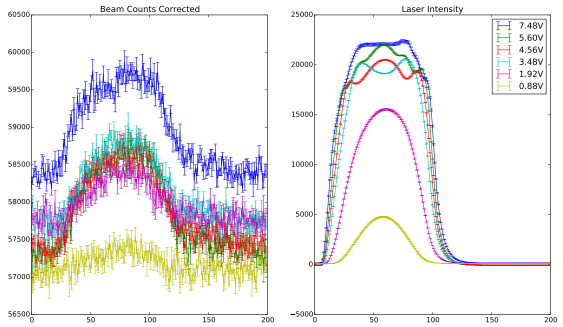

Fig. 10: Left: beam counts for different chopper amplitudes. Right: laser intensity as measured through the chopper. At higher amplitudes the signal clearly displays higher harmonics. The data was recorded at mounting hole 27, at a cold-head temperature of 20K.

However, when using the photo-diode signal as the chopper function, the problem of large uncertainties in the fit parameters is solved. Furthermore, when calculating the temperature of the beam the photo-diode method gives a result which is consistent with the known properties of the beam.

To conclude, it appears that using the photo-diode signal to perform the fitting is the preferred method.

III. Outlook

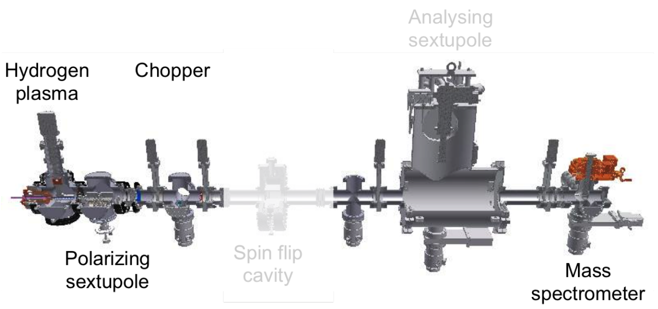

Fig. 11: Stage 2. The complete setup except for the spin-flip cavity. This setup will be used to characterize the analyzing sextupoles.

The next stage is the whole setup but without the spin flip cavity, shown in Figure 11. The goal with this stage is the characterization of the analyzing sextupole. After this has been installed the mounting hole scan should also be repeated to see if this solves the problem of no apparent dependence.

A big difference between the setup as illustrated and the final setup is the replacement of the superconducting sextupole by several permanent ones. Characterization of the permanent sextupoles will be the topic of future research.

IV. Conclusion

It was found that a Gaussian distribution matches the beam shape better than a Maxwell-Boltzmann distribution. However, the evidence is not very convincing as the χ^2 for both models is roughly the same.

For the chopper function it is better to use the photo-diode signal, if available. When no laser is available a peak to peak voltage voltage of about 3.48 V is suggested.

A mounting hole dependence for the velocity is predicted by simulation and previous measurements with the full setup, but could not be confirmed with the short setup. Furthermore, there does not even seem to be a dependence on source temperature. Further analysis of the data and scrutiny of the ROOT code used for fitting is needed.

V. Acknowledgments

I would like to thank Chloé Malbrunot for giving me the opportunity to work in this group. Furthermore I would like to thank Martin Simon and Oswald Massiczek for their guidance.

References

[1] M. Diermaier, P. Caradonna, B. Kolbinger, C. Malbrunot, O. Massiczek, C. Sauerzopf, M. C. Simon, M. Wolf, J. Zmeskal, and E. Widmann. An atomic hydrogen beam to test ASACUSA's apparatus for antihydrogen spectroscopy. *Hyperfine Interactions*, 233:35–40, August 2015.

[2] N. Kuroda, S. Ulmer, D. J. Murtagh, S. Van Gorp, Y. Nagata, M. Diermaier, S. Federmann, M. Leali, C. Malbrunot, V. Mascagna, O. Massiczek, K. Michishio, T. Mizutani, A. Mohri, H. Nagahama, M. Ohtsuka, B. Radics, S. Sakurai, C. Sauerzopf, K. Suzuki, M. Tajima, H. A. Torii, L. Venturelli, B. Wünschek, J. Zmeskal, N. Zurlo, H. Higaki, Y. Kanai, E. Lodi Rizzini, Y. Nagashima, Y. Matsuda, E. Widmann, and Y. Yamazaki. A source of antihydrogen for in-flight hyperfine spectroscopy. *Nat Commun*, 5, 01 2014.

[3] C. Malbrunot et al. Spectroscopy Apparatus for the Measurement of the Hyperfine Structure of Antihydrogen. *Hyperfine Interact.*, 228(1-3):61–66, 2014.